Laser-Based Kinematic Calibration of Robot Manipulator Using Differential Kinematics

In-Won Park, Bum-Joo Lee, Se-Hyoung Cho, Young-Dae Hong, and Jong-Hwan Kim, *Fellow, IEEE*

***Abstract*—This paper proposes a novel systematic technique to estimate entire kinematic parameter errors of robot manipulator. Small errors always exist in link length and link twist for physical manipulators, which affect the precision in kinematic equations leading to calculate wrong joint angle values in inverse kinematic equations. In order to solve these problems, the proposed technique employs a structured laser module (SLM), a stationary camera, the Jacobian matrices, and an extended Kalman filter (EKF). The SLM is attached to the end-effector of the manipulator arm and the stationary camera is used to determine an accurate position where the laser comes out. Variances between actual and measured positions of laser beams are represented by the Jacobian matrices formulated from differential kinematics. Then, the EKF is used to estimate kinematic parameters. Effectiveness of the proposed technique is verified with 7 DOF humanoid manipulator arm by computer simulation and 4 DOF manipulator by actual experiment.**

***Index Terms*—Differential kinematics, extended Kalman filter (EKF), kinematic calibration, structured laser module (SLM).**

I. Introduction

THE geometry of a robot manipulator commonly does not match the designed goals, which reduces the accuracy of the end-effector location significantly. Inaccuracies in kinematic parameters of the robot manipulator arise from two types of errors: geometric and nongeometric errors. The geometric errors are due to inaccurate knowledge of the kinematic model, and the nongeometric errors are caused by joint and link compliances, thermal, wear, etc. In order to operate the humanoid robot [1], [2] or to move the manipulator arm [3] and robot finger [4] to a specified location consistently and accurately, a kinematic calibration is required because the location of the manipulator is based on a precise description of the kinematic parameters.

There were many pieces of research related to the kinematic identification and calibration of the robot manipulator [5]–[8]. A methodology that uses laser was introduced to capture robot position data in order to model stiffness of the robot manipulator [9] and to predict kinematic parameters [10]–[14]. O'Brian *et al.* also employed a magnetic motion capture data to determine the kinematic parameters [15]. Renaud *et al.* [16] and Rauf *et al.* [17] used a vision-based measuring device and a partial pose measurement device for kinematic calibration of parallel mechanisms, respectively. Gatti and Danieli demonstrated a pose-matching procedure for calibration, which provides a low-cost and easy-to-use external metrology system [18]. Santolaria *et al.* recently demonstrated a continuous data capture technique by using a ball bar gauge and a coupling probe to estimate kinematic parameters of articulated arm coordinated measuring machines [19]. It was concluded that the parameter error was minimized in the measured positions, whereas the error increased in very different positions because the optimization technique was only based on the position information of end-effector. To overcome this problem, Ye *et al.* [20] and Iurascu and Park [21] demonstrated a kinematic calibration method using differential kinematics and iterative algorithms to determine parameters. The radial basis function network was chosen as an optimization algorithm [22], where the Gauss–Newton and Levenberg–Marquardt methods were applied as identification approaches [23]. Daney *et al.* also introduced an algorithm that selected the minimum number of necessary positions in order to obtain reliable results following optimization [24].

In this paper, a novel systematic technique is proposed to estimate entire kinematic parameter errors of the robot manipulator by using a structured laser module (SLM), a stationary camera, the Jacobian matrices, and an extended Kalman filter (EKF). Kinematic calibration techniques generally consist of four processes: kinematic modeling, measurement, estimation, and correction. The Denavit–Hartenberg (D–H) convention is used as kinematic modeling because it has a minimal representation for the common normal between two revolute links [25]. The SLM made with two laser sources is attached to the end-effector and beamed onto the screen, where the stationary camera is used to measure the exact positions of these laser beams.

The contribution of this paper is to formulate a nonsingular Jacobian matrix, which represents how each kinematic parameter error influences the variance between the theoretical and measured positions of laser beams on the screen. The proposed technique derives two Jacobian matrices: the relationship between the differential joint displacements and the end-effecter location including its position and orientation, and the relationship between the velocity of end-effector and the laser beamed onto the screen. If these two Jacobian matrices are multiplied, the Jacobian matrix representing the differential motion of individual joints and the laser location is formulated. By using a set of laser beam measurements and a set of corresponding joint values, EKF is iterated to estimate differential errors of individual kinematic parameters. The proposed estimation

Manuscript received March 4, 2011; revised May 6, 2011; accepted May 16, 2011. Date of publication June 30, 2011; date of current version August 24, 2012. Recommended by Technical Editor J. M. Berg. This work was supported by the Basic Science Research Program through the National Research Foundation of Korea funded by the Ministry of Education, Science, and Technology under Grant 2011-0000321.

I.-W. Park, S.-H. Cho, Y.-D. Hong, and J.-H. Kim are with the Department of Electrical Engineering, Korea Advanced Institute of Science and Technology (KAIST), Daejeon 305-701, Korea (e-mail: iwpark@rit.kaist.ac.kr; shcho@rit.kaist.ac.kr; ydhong@rit.kaist.ac.kr; johkim@rit.kaist.ac.kr).

B.-J. Lee is with the Digital Media and Communications R&D Center, Samsung Electronics, Suwon 443-742, Korea (e-mail: leebumjoo@gmail.com).

Color versions of one or more of the figures in this paper are available online at http://ieeexplore.ieee.org.

Digital Object Identifier 10.1109/TMECH.2011.2158234

technique is verified with 7 DOF humanoid arm by simulation and 4 DOF manipulator by actual experiment. Simulation and actual experimental results confirm that the proposed technique estimates the true errors existing in individual kinematic parameters and minimizes the distance errors between the theoretical and measured positions of the laser beams on the screen.

This paper is organized as follows. Section II describes the problem definition including the kinematic equation and the SLM. Section III proposes a systematic technique to estimate kinematic parameters using the stationary camera, the Jacobian formulation, and the EKF. Sections IV and V present the simulation results of a 7 DOF manipulator arm and the experimental results of a 4 DOF manipulator, respectively, to verify the effectiveness of the proposed estimation technique. Concluding remarks follow in Section V.

II. Problem Definition

To examine all the geometrical and time-based properties of manipulator motions, it is essential to have an accurate measurement of manipulator kinematics. However, there always exist small errors in link lengths and link twists for physical manipulators. These errors eventually affect the precision in kinematic equations, and cause inverse kinematic equations to calculate joint angle values with errors. Thus, the objective of this paper is to determine the physical errors of all kinematic parameters in order to obtain accurate kinematic and inverse kinematic equations. This section describes the formulation of the kinematic model and the SLM.

Manipulator kinematics is represented by the D–H method, which consists of four link parameters: link length a, link offset d, link twist α, and joint angle θ. The geometrical significance of using the D–H method is that it avoids redundancies and perfectly describes manipulator kinematics, where mutual perpendicular axes always exist between two consecutive revolute joints. Assuming that the two revolute links described in frames $\{i-1\}$ and $\{i\}$ are perfectly aligned, the transformation matrix $\mathbf{T}$ is defined as follows:

$$
\begin{aligned}
{}^{i-1}_{i}\mathbf{T} &= \mathrm{Trans}\,(x,a)\,\mathrm{Trans}\,(z,d)\,\mathrm{Rot}\,(x,\alpha)\,\mathrm{Rot}\,(z,\theta) \\
&= \begin{bmatrix} c(\theta) & -s(\theta) & 0 & a \\ c(\alpha)\,s(\theta) & c(\alpha)\,c(\theta) & -s(\alpha) & 0 \\ s(\alpha)\,s(\theta) & s(\alpha)\,c(\theta) & c(\alpha) & d \\ 0 & 0 & 0 & 1 \end{bmatrix} \qquad (1)
\end{aligned}
$$

where Trans and Rot correspond to translation and rotation, and cos and sin are abbreviated to c and s, respectively. However, in physical manipulators, links are generally misaligned due to small errors in the parameters of the D–H notation and the corresponding transformation matrix is modified as follows:

$$
\begin{aligned}
{}^{i-1}_{i}\mathbf{T} &= \mathrm{Trans}\,(x,a+\Delta a)\,\mathrm{Trans}\,(z,d+\Delta d) \\
&\quad \mathrm{Rot}\,(x,\alpha+\Delta\alpha)\,\mathrm{Rot}\,(z,\theta+\Delta\theta) \qquad (2)
\end{aligned}
$$

where Δa, Δd, $\Delta\alpha$, and $\Delta\theta$ represent the physical differential errors of link length, link offset, link twist, and joint angle, respectively.

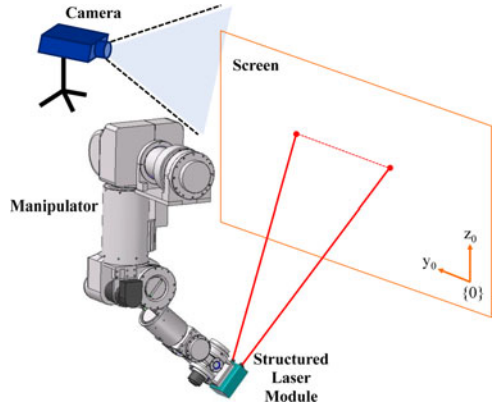

Fig. 1. Kinematic calibration technique using an SLM and stationary camera.

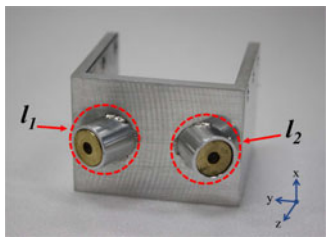

Fig. 2. SLM having two laser sources (l_1 and l_2).

Fig. 1 shows the configuration of the proposed system, which consists of the manipulator arm having an SLM, a stationary camera, and a screen. Note that the base frame $\{0\}$ is located on the screen and the stationary camera is used to measure an accurate position of the two lasers on the screen. If we have an accurate knowledge of the D–H parameters in relation to the manipulator, then the position of the two laser beams on the screen must be equivalent to the solution of kinematic equations. However, this situation is commonly impracticable due to the presence of physical errors shown in (2). Thus, this paper proposes a novel kinematic calibration technique to estimate the true errors existing in individual D–H parameters and to minimize the variances between the theoretical and measured positions of laser beams.

In the proposed technique, the SLM made with two laser sources is attached to the end-effector of the manipulator, which is used to measure an accurate position of the end-effector. Fig. 2 shows the image of the SLM used in the experiment, where two transformation matrices from the SLM to each laser source, l_1 and l_2, are defined as follows:

$$
\begin{aligned}
{}^{\mathrm{SLM}}_{l_1}\mathbf{T} &= \mathrm{Rot}\,(x,-30.0^\circ) \\
{}^{\mathrm{SLM}}_{l_2}\mathbf{T} &= \mathrm{Rot}\,(x,30.0^\circ)\,. \qquad (3)
\end{aligned}
$$

Note that the direction of the x-axis is pointed upward of the SLM. There exist physical offset errors in these rotation angles during the manufacturing process as well. These error values will be found separately before attaching to the last link of the manipulator. A detailed procedure of finding the accurate rotation angles of the SLM is described in Section V.

Based on the aforementioned information, two kinematic equations representing the relationship between the base frame and each of the laser sources are formed by multiplying the individual link-transformation matrices together as follows:

$$
{}^{0}_{l_i}\mathbf{T} = {}^{0}_{1}\mathbf{T}\,{}^{1}_{2}\mathbf{T}\,{}^{2}_{3}\mathbf{T}\cdots{}^{N-1}_{N}\mathbf{T}\,{}^{N}_{\mathrm{SLM}}\mathbf{T}\,{}^{\mathrm{SLM}}_{l_i}\mathbf{T} = \begin{bmatrix} \mathrm{x}_x & \mathrm{y}_x & \mathrm{z}_x & \mathrm{p}_x \\ \mathrm{x}_y & \mathrm{y}_y & \mathrm{z}_y & \mathrm{p}_y \\ \mathrm{x}_z & \mathrm{y}_z & \mathrm{z}_z & \mathrm{p}_z \\ 0 & 0 & 0 & 1 \end{bmatrix}
$$

$$
= \begin{bmatrix} \mathbf{x} & \mathbf{y} & \mathbf{z} & \mathbf{p} \\ 0 & 0 & 0 & 1 \end{bmatrix} = \begin{bmatrix} {}^{0}_{l_i}\mathbf{R} & & & \mathbf{p} \\ 0 & 0 & 0 & 1 \end{bmatrix}, \quad i = 1, 2 \tag{4}
$$

where N represents the total number of joints and ${}^{0}_{l_i}\mathbf{R}$ describes the rotation matrix in frame $\{l_i\}$ relative to frame $\{0\}$. According to [6], the number of geometric parameters for completeness is $4R + 2P + 6$, where R and P represent the number of revolute and prismatic joints, respectively. In our case, the translation error along the direction of a laser beam (y-axis of the SLM) cannot be measured. Even if there is an error in this direction, it does not affect any variation on the screen, where the laser beam is projected. Since there are four parameters for N revolute joints and five parameters (two positions and three orientations) for the SLM, the number of total parameters to be considered becomes $4N + 5$.

Due to the position and angle at which the camera is mounted and the lens distortion, distorted images from the stationary camera must be corrected. The image calibration algorithm for the robot soccer system, which is realized by authors, is used to find the exact position of the two laser beams on the screen. This algorithm returns the measured position of the two laser beams with respect to the base frame $\{0\}$.

III. Kinematic Calibration Using Differential Kinematics

In order to estimate physical offset errors in D–H parameters, this paper proposes a novel kinematic calibration technique by using Jacobian matrices derived from the differential kinematics and the EKF. Two Jacobian matrices, one that relates differential velocities of individual joints to the Cartesian velocities of the end-effector and the other that relates the Cartesian velocities of the end-effector to the laser velocities on the screen, are derived. Then, the EKF is explained, which is used as an optimization tool to estimate link parameters.

A. Jacobian Formulation

The Jacobian matrix that relates joint velocities to end-effector velocities can be directly found by differentiating the kinematic equations. However, this process returns only 3×1 linear velocity vector and no 3×1 rotation velocity vector. Thus, the velocity vector of the differential motion for each link has to be computed in order, starting from the base frame.

The differential motion transform describes a small motion of an object in space. This small differential motion causes the errors between the theoretical and measured positions of the laser beams on the screen. Thus, the concept of differential motion is applied to estimate the errors in the geometric model parameters [28]. Transformation of differential motion from frame $\{1\}$ to frame $\{l\}$ can be expressed as a 6×4 matrix as follows:

$$
\begin{bmatrix} {}^{l}\partial v_x \\ {}^{l}\partial v_y \\ {}^{l}\partial v_z \\ {}^{l}\partial w_x \\ {}^{l}\partial w_y \\ {}^{l}\partial w_z \end{bmatrix} = {}^{1}\mathbf{J}(\Delta) \begin{bmatrix} {}^{1}\partial v_x \\ {}^{1}\partial v_z \\ {}^{1}\partial w_x \\ {}^{1}\partial w_z \end{bmatrix} \tag{5}
$$

with

$$
{}^{1}\mathbf{J}(\Delta) = \begin{bmatrix} \mathrm{x}_x & \mathrm{z}_x & \left(({}^{l}\mathbf{p} - {}^{1}\mathbf{p}) \times \mathbf{x}\right)_x & \left(({}^{l}\mathbf{p} - {}^{1}\mathbf{p}) \times \mathbf{z}\right)_x \\ \mathrm{x}_y & \mathrm{z}_y & \left(({}^{l}\mathbf{p} - {}^{1}\mathbf{p}) \times \mathbf{x}\right)_y & \left(({}^{l}\mathbf{p} - {}^{1}\mathbf{p}) \times \mathbf{z}\right)_y \\ \mathrm{x}_z & \mathrm{z}_z & \left(({}^{l}\mathbf{p} - {}^{1}\mathbf{p}) \times \mathbf{x}\right)_z & \left(({}^{l}\mathbf{p} - {}^{1}\mathbf{p}) \times \mathbf{z}\right)_z \\ 0 & 0 & \mathrm{x}_x & \mathrm{z}_x \\ 0 & 0 & \mathrm{x}_y & \mathrm{z}_y \\ 0 & 0 & \mathrm{x}_z & \mathrm{z}_z \end{bmatrix}
$$

where v and w represent the linear and rotational velocities, respectively. This 6×4 matrix is denoted as ${}^{1}\mathbf{J}(\Delta)$, in which the values of each component can be directly found by using the transformation matrix. Note that there is no linear or rotational velocity component on the y-axis because the D–H notation does not have any translation and rotation on the y-axis. The order of the linear and rotational velocities in (5) is equivalent to the order of the derivative of D–H parameters in (1).

In this manner, the Jacobian matrix that relates the differential motion of individual joints to the end-effector, denoted as $\mathbf{Jac}_1$, can be defined as follows:

$$
\mathbf{Jac}_1 = \left[\, {}^{1}\mathbf{J}\,(\Delta)\, {}^{2}\mathbf{J}\,(\Delta) \cdots {}^{N}\mathbf{J}\,(\Delta)\, {}^{\mathrm{SLM}}\mathbf{J}\,(\Delta) \,\right]. \tag{6}
$$

Next is to find the relationship between the end-effector and the laser that is beamed onto the screen. The position and velocity vectors between the laser source that is attached to the SLM and the screen can be represented as follows:

$$
{}^{0}\mathbf{p} = {}^{l}\mathbf{p} + {}^{0}_{l}\mathbf{R} \begin{bmatrix} 0 \\ 0 \\ 1 \end{bmatrix} k
$$

$$
{}^{0}\dot{\mathbf{p}} = {}^{l}\dot{\mathbf{p}} + \begin{bmatrix} w_x \\ w_y \\ w_z \end{bmatrix} \times \left({}^{0}_{l}\mathbf{R} \begin{bmatrix} 0 \\ 0 \\ 1 \end{bmatrix} k \right) + {}^{0}_{l}\mathbf{R} \begin{bmatrix} 0 \\ 0 \\ 1 \end{bmatrix} \dot{k} \tag{7}
$$

where k and $\dot{k}$ are constants, which represent the distance and the velocity between the laser source on SLM and the laser beam on screen, respectively. Note that (7) describes a general transformation mapping of the position and velocity vectors from its description in the frame $\{l\}$ to the description in the frame $\{0\}$. Since the screen is equivalent to the base frame $\{0\}$, as shown in Fig. 1, x-component of the position vector in the frame $\{0\}$ becomes 0 and the value of k can be calculated as follows:

$$
{}^{0}\mathrm{p}_x = {}^{l}\mathrm{p}_x + \mathrm{z}_x k = 0
$$

$$
k = -\frac{{}^{l}\mathrm{p}_x}{\mathrm{z}_x}. \tag{8}
$$

Similarly, x-component of the velocity vector on the screen is 0 and the value of $\dot{k}$ can be calculated by substituting (8) as follows:

$$
\begin{aligned}
{}^{0}\dot{\mathrm{p}}_x &= {}^{l}\dot{\mathrm{p}}_x + (w_y \mathrm{z}_z - w_z \mathrm{z}_y)\, k + \mathrm{z}_x \dot{k} = 0 \\
\dot{k} &= -\frac{{}^{l}\dot{\mathrm{p}}_x \mathrm{z}_x - (w_y \mathrm{z}_z - w_z \mathrm{z}_y)\, {}^{l}\mathrm{p}_x}{\mathrm{z}_x^2}.
\end{aligned} \tag{9}
$$

In this manner, the two equations that relate the end-effector velocities to the point laser velocities on the screen are given by

$$
\begin{aligned}
{}^{0}\dot{\mathrm{p}}_y &= {}^{l}\dot{\mathrm{p}}_y + (w_z \mathrm{z}_x - w_x \mathrm{z}_z)\, k + \mathrm{z}_y \dot{k} = 0 \\
{}^{0}\dot{\mathrm{p}}_z &= {}^{l}\dot{\mathrm{p}}_z + (w_x \mathrm{z}_y - w_y \mathrm{z}_x)\, k + \mathrm{z}_z \dot{k} = 0.
\end{aligned} \tag{10}
$$

Substituting (8) and (9) into (10), we obtain

$$
\begin{bmatrix} {}^{0}\partial v_y \\ {}^{0}\partial v_z \end{bmatrix} = \mathbf{Jac}_2 \begin{bmatrix} {}^{l}\partial v_x \\ {}^{l}\partial v_y \\ {}^{l}\partial v_z \\ {}^{l}\partial w_x \\ {}^{l}\partial w_y \\ {}^{l}\partial w_z \end{bmatrix} \tag{11}
$$

with

$$
\mathbf{Jac}_2 = \begin{bmatrix}
-\dfrac{\mathrm{z}_y}{\mathrm{z}_x} & 1 & 0 & \dfrac{\mathrm{z}_z\, {}^{l}\mathrm{p}_x}{\mathrm{z}_x} & \dfrac{\mathrm{z}_z \mathrm{z}_y\, {}^{l}\mathrm{p}_x}{\mathrm{z}_x^2} & -\dfrac{\left(1-\mathrm{z}_z^2\right) {}^{l}\mathrm{p}_x}{\mathrm{z}_x^2} \\
-\dfrac{\mathrm{z}_z}{\mathrm{z}_x} & 0 & 1 & -\dfrac{\mathrm{z}_y\, {}^{l}\mathrm{p}_x}{\mathrm{z}_x} & \dfrac{\left(1-\mathrm{z}_y^2\right) {}^{l}\mathrm{p}_x}{\mathrm{z}_x^2} & -\dfrac{\mathrm{z}_z \mathrm{z}_y\, {}^{l}\mathrm{p}_x}{\mathrm{z}_x^2}
\end{bmatrix}
$$

where this 2×6 matrix is denoted as $\mathbf{Jac}_2$, which represents the Jacobian matrix that relates the end-effector velocities to the laser velocities on the screen.

The Jacobian matrix $\mathbf{J}$ that relates joint velocities of each link to the point laser velocities on the screen for the two laser sources l_1 and l_2 attached to the end-effector is formulated by multiplying the values of $\mathbf{Jac}_1$ and $\mathbf{Jac}_2$ as

$$
\mathbf{J} = \begin{bmatrix} {}^{l_1}\mathbf{Jac}_2^{l_1}\mathbf{Jac}_1 \\ {}^{l_2}\mathbf{Jac}_2^{l_2}\mathbf{Jac}_1 \end{bmatrix}. \tag{12}
$$

The Jacobian matrix in (12) will be utilized in the EKF algorithm presented in the following section.

In summary, the proposed technique derives the Jacobian matrices using the concept of differential motion. These Jacobian matrices consider not only the final location of the SLM, but also the velocity at which the SLM moves. In other words, the differential motion of individual joints that influence the direction and speed of SLM is represented by the Jacobian matrix, $\mathbf{Jac}_1$. Then, the motion of the SLM in the joint space and the base frame is represented by $\mathbf{Jac}_2$. Due to the formulation of these Jacobian matrices, the proposed technique allows us to estimate the physical errors existing in the entire kinematic parameters with a small number of measurements.

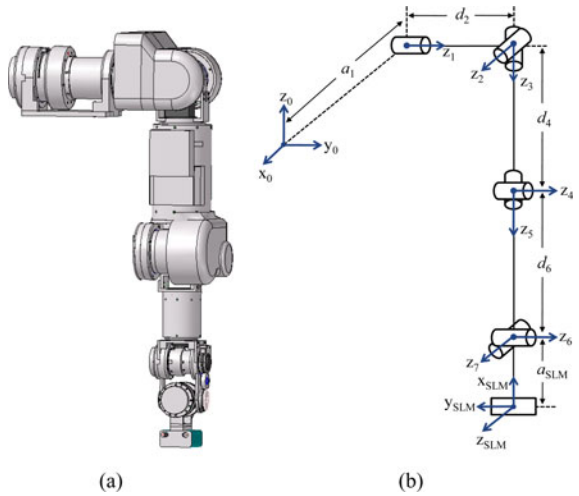

Fig. 3. 7 DOF humanoid arm. (a) Snapshot of humanoid arm having SLM. (b) D–H parameters and frame assignments. Note that the frame $\{0\}$ is located on the screen.

TABLE I
NOMINAL VALUES OF D–H PARAMETER FOR HUMANOID ARM

Joint	a (mm)	d (mm)	α (°)	θ (°)	Range (°)
1	-500.0	0.0	-90.0	$\theta_1 - 90.0$	-180.0 to 90.0
2	0.0	100.0	-90.0	$\theta_2 + 90.0$	-10.0 to 90.0
3	0.0	0.0	-90.0	$\theta_3 - 90.0$	-10.0 to 30.0
4	0.0	200.0	90.0	θ_4	-120.0 to 0.0
5	0.0	0.0	-90.0	θ_5	-90.0 to 90.0
6	0.0	200.0	90.0	$\theta_6 + 90.0$	-30.0 to 30.0
7	0.0	0.0	90.0	θ_7	-30.0 to 30.0
SLM	50.0	0.0	0.0	180.0	0.0

B. Extended Kalman Filter

Initially, the positions of the two laser beams for the specified number of poses are observed from a 2-D screen and captured by the stationary camera. Since uncertainty exists in the measurement, EKF is used as an optimization algorithm and the Jacobian matrices are applied to estimate the accurate errors of D–H parameters by using these measured position values [26], [27].

In the prediction step of the Kalman filter, the predicted state $\hat{\mathbf{x}}$ is $4N + 5$ offset errors of D–H parameters for the manipulator. The covariance matrix of the predicted state $\mathbf{P}$ can be obtained as follows:

$$
\begin{aligned}
\hat{\mathbf{x}}_{k+1|k} &= \hat{\mathbf{x}}_{k|k} \\
\mathbf{P}_{k+1|k} &= \mathbf{P}_{k|k} + \mathbf{Q}_k
\end{aligned} \tag{13}
$$

where $\mathbf{Q}$ is the covariance matrix of the system noise. In the observation step of the Kalman filter, Jacobian matrix $\mathbf{J}$, measurement residual $\tilde{\mathbf{y}}$, and residual covariance $\mathbf{S}$ are calculated as follows:

$$
\begin{aligned}
\mathbf{J}_{k+1} &= \left.\frac{\partial \mathbf{T}(x)}{\partial x}\right|_{\hat{\mathbf{x}}_{k+1|k}} \\
\tilde{\mathbf{y}}_{k+1} &= \mathbf{m}_{k+1} - \mathbf{T}(\hat{\mathbf{x}}_{k+1|k}) \\
\mathbf{S}_{k+1} &= \mathbf{J}_{k+1}\mathbf{P}_{k+1|k}\mathbf{J}_{k+1}^{T} + \mathbf{R}_{k+1}
\end{aligned} \tag{14}
$$

where $\mathbf{m}$ is the measured position of the point laser on the screen and $\mathbf{R}$ is the covariance matrix of measurement noise. Note that

TABLE II
DISTANCE ERRORS OF TWO LASER BEAMS ON THE SCREEN BEFORE THE CALIBRATION PROCEDURE (SIMULATION)

	Calibration Set (mm)							Testing Set (mm)						
		l_1			l_2				l_1			l_2		
	Poses	Mean	STD	Max	Mean	STD	Max	Poses	Mean	STD	Max	Mean	STD	Max
Case 1	30	84.06	4.54	96.03	15.94	6.83	29.11	30	89.16	20.48	154.18	29.73	19.63	85.49
Case 2	30	84.34	15.62	154.18	27.07	18.70	85.49	30	88.88	14.10	143.93	18.59	11.89	55.34
Case 3	60	86.61	15.05	154.18	22.83	16.24	85.49	-	-	-	-	-	-	-

TABLE III
DISTANCE ERRORS OF TWO LASER BEAMS ON THE SCREEN AFTER THE CALIBRATION PROCEDURE (SIMULATION)

		Calibration Set (mm)							Testing Set (mm)						
			l_1			l_2				l_1			l_2		
		Poses	Mean	STD	Max	Mean	STD	Max	Poses	Mean	STD	Max	Mean	STD	Max
LSE	Case 1	30	0.42	0.14	0.79	0.32	0.13	0.62	30	0.77	0.52	2.19	0.82	0.57	2.98
	Case 2	30	0.18	0.13	0.49	0.15	0.10	0.53	30	0.22	0.19	0.81	0.20	0.17	0.72
	Case 3	60	0.15	0.10	0.47	0.12	0.09	0.44	-	-	-	-	-	-	-
EKF	Case 1	30	0.12	0.04	0.23	0.08	0.04	0.16	30	0.27	0.14	0.69	0.29	0.13	0.65
	Case 2	30	0.09	0.05	0.26	0.09	0.06	0.25	30	0.09	0.06	0.27	0.09	0.06	0.28
	Case 3	60	0.10	0.06	0.29	0.08	0.06	0.23	-	-	-	-	-	-	-

$k+1|k$ means a prior estimate, where $k+1|k+1$ denotes *a posteriori* estimate.

Last step of the Kalman filter is to update the values of the state and the state covariance matrix by calculating an optimal Kalman gain $\mathbf{K}$ as follows:

$$\begin{aligned}\mathbf{K}_{k+1} &= \mathbf{P}_{k+1|k}\mathbf{J}_{k+1}^{T}\mathbf{S}_{k+1}^{-1}\\ \hat{\mathbf{x}}_{k+1|k+1} &= \hat{\mathbf{x}}_{k+1|k} + \mathbf{K}_{k+1}\tilde{\mathbf{y}}_{k+1}\\ \mathbf{P}_{k+1|k+1} &= (\mathbf{I} - \mathbf{K}_{k+1}\mathbf{J}_{k+1})\mathbf{P}_{k+1|k}\end{aligned} \tag{15}$$

where $\mathbf{I}$ is the identity matrix. Once the updating procedure is completed, norm values of the state vector and measured positions are calculated for every iteration. Then, the aforementioned three steps are iterated until these norm values converge to certain desired values, which are defined by the user. Note that if $\mathbf{Q}$ and $\mathbf{R}$ are set to zero, then EKF simply reduces to the Newton–Raphson method.

IV. SIMULATION RESULTS

A. Simulation Setup

The humanoid arm having 7 DOF was used in the simulation. Fig. 3 shows the snapshot, D–H parameters, and frame assignments of the humanoid arm, where the nominal values of the D–H parameters are summarized in Table I. Since the elbow joint cannot bend backward from its initial configuration, the value of θ_4 was always set as a negative value. For EKF, the number of maximum iteration was set as 5000, and both $\mathbf{Q}$ and $\mathbf{R}$ were set as $1.0 \times 10^{-4}\mathbf{I}_{33}$. The iteration terminated when the norm value of the state vector was less than 1.0×10^{-7}.

The error values of all the D–H parameters were set as (Δa, Δd, $\Delta\alpha$, $\Delta\theta$) = (10.0 mm, 10.0 mm, 1.0°, 1.0°). The random noise of $[-0.1^\circ, 0.1^\circ]$ was added as a bounded error of joint disturbance. In addition, when the positions of the two laser beams on the screen were measured, the random measurement noise of [-2.0 mm, 2.0 mm] was added to consider the optical diffraction of the laser beams on the screen.

B. Results

To verify the effectiveness of the proposed algorithm, laser positions of a total of 60 poses were measured. The joint values for the first 30 poses were chosen between -10.0° and 10.0° and the others were chosen over the whole operating workspace shown in Table I. In Case 1, the former 30 poses were used as the calibration set and the latter 30 poses were used as the testing set. In Case 2, a half of the calibration and the testing set used in Case 1 was used as the calibration set, and the other half was used as the testing set. This way, the calibration set for Case 1 only contained the poses covering a small range of workspace, whereas Case 2 included the poses covering the whole workspace. In Case 3, the complete set of 60 poses were used as the calibration set.

The proposed algorithm was evaluated by calculating the distance between the measured positions of the two laser beams and the theoretical position obtained by using (7). Table II shows the distance errors of the two laser beams on the screen for each case before the calibration procedure, which includes the mean distance error, the standard deviation, and the maximum distance error. In Case 3, which contains the complete set, the average distance error for l_1 was 86.61 mm with the standard deviation of 15.05 and 154.18 mm as the maximum error value. The average distance error for l_2 was 22.83 mm with the standard deviation of 16.24 and 85.49 mm as the maximum error value.

Table III presents the distance errors of the two laser beams on the screen after the calibration procedure. The performance of the proposed algorithm was compared to that of the least-squares estimation (LSE) method, which is the fast and computationally efficient identification algorithm [18]. When the estimated D–H parameter error values were added to the nominal values, shown in Table I, the mean distance errors of calibration set for all three cases were less than 1.0 mm. Note that the maximum distance errors of the calibration set for all three cases were smaller than the measurement noise, which was ± 2.0 mm. The results of the testing set in both Case 1 and Case 2 confirmed that EKF significantly enhanced the overall performance of the proposed algorithm compared to LSE. In addition, the distance errors between the theoretical and measured positions of the two laser beams decreased when the calibration set included the poses that covered the whole workspace.

Fig. 4 shows the estimated D–H parameter error values of the humanoid arm when the calibration set of Case 1 was used in EKF. As shown in Fig. 4, the proposed algorithm quickly

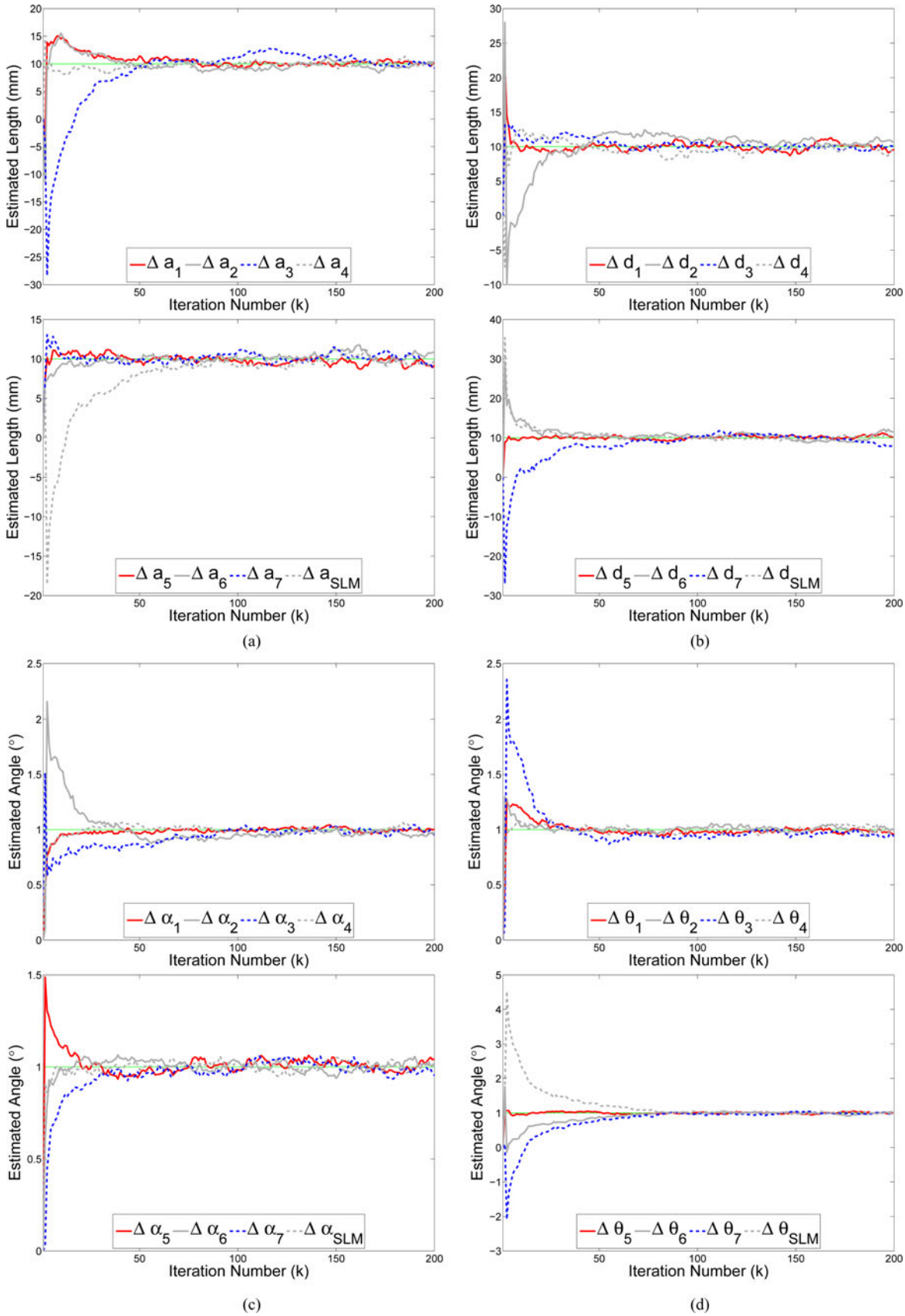

Fig. 4. Estimated D–H parameter errors of humanoid arm for Case 1 when EKF is used as an optimization algorithm (simulation). (a) Estimated link length. (b) Estimated link offset. (c) Estimated link twist. (d) Estimated joint disturbance.

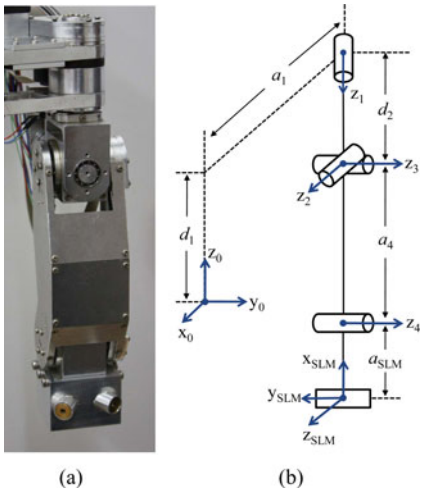

Fig. 5. 4 DOF manipulator. (a) Snapshot of manipulator having SLM. (b) D–H parameters and frame assignments. Note that the frame $\{0\}$ is located on the screen.

TABLE IV
NOMINAL VALUES OF THE D–H PARAMETER FOR 4 DOF MANIPULATOR

Joint	a (mm)	d (mm)	α (°)	θ (°)	Range (°)
1	-365.0	690.0	0.0	$\theta_1 - 90.0$	-30.0 to 30.0
2	0.0	-30.0	-90.0	$\theta_2 + 90.0$	-20.0 to 20.0
3	0.0	0.0	-90.0	θ_3	-90.0 to 45.0
4	100.0	0.0	0.0	$\theta_4 + 180.0$	-60.0 to 90.0
SLM	-30.0	0.0	-90.0	0.0	0.0

converged to the true error values defined by the user. The norm value of 33 parameters for all three cases was less than 0.01 within 100 iterations in EKF. Note that the positions of the laser beams on the screen perfectly matched the theoretical positions when the joint disturbances and the measurement noises were not added in the simulation environment.

V. EXPERIMENTAL RESULTS

A. Experimental Setup

The 4 DOF manipulator was used in the experiment, which consists of four dc motors with harmonic drives to provide control accuracy, gear reduction, and sufficient power. Fig. 5 shows a snapshot, D–H parameters, and frame assignments of the manipulator. The nominal values of the D–H parameters and operating ranges are summarized in Table IV. Due to the characteristic of the dc motor with the harmonic drive, the gear backlashs and transmission errors for each joint were minimized. The joint values had the accuracy of one-tenth of a degree and the diffraction length of the two laser beams were approximately 4.0 mm. The number of maximum iteration was set as $10\,000$, and both $\mathbf{Q}$ and $\mathbf{R}$ were set as $1.0 \times 10^{-4}\mathbf{I}_{21}$ for EKF.

Before attaching the SLM to the end-effector of the manipulator, the accurate rotation angles of the two laser sources must be found because there are physical offset errors during the manufacturing process. Fig. 6 shows the calibration procedure of the SLM. The actual transformation matrices from the SLM to each laser source, l_1 and l_2, were founded by using the trigonometric functions as follows:

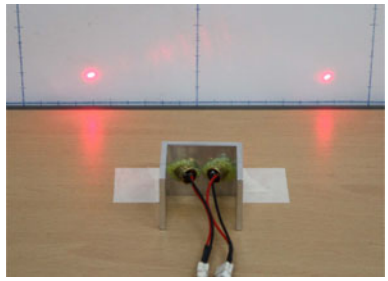

Fig. 6. Calibrating the rotation angles from an SLM to a laser source.

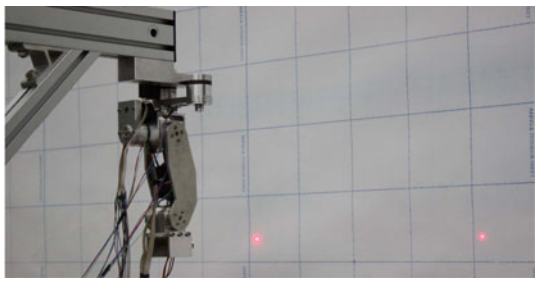

Fig. 7. Snapshot of manipulator and two laser beams on the screen at the initial configuration.

TABLE V
ESTIMATED PARAMETER ERRORS OF 4 DOF MANIPULATOR USING THE CALIBRATION SET (EXPERIMENT)

		Case 1	Case 2	Case 3
1	Δa_1 (mm)	-0.0653	-0.0453	-0.0088
2	Δd_1 (mm)	0.7499	0.0788	0.0028
3	$\Delta\alpha_1$ (°)	0.0859	-0.4756	-0.3953
4	$\Delta\theta_1$ (°)	0.1042	-0.0844	-0.0688
5	Δa_2 (mm)	0.0567	-0.0463	-0.0359
6	Δd_2 (mm)	-0.6759	-0.0411	-0.0047
7	$\Delta\alpha_2$ (°)	-0.1337	-0.1155	-0.0972
8	$\Delta\theta_2$ (°)	-0.0141	0.0087	0.0115
9	Δa_3 (mm)	0.0724	0.0355	0.0346
10	Δd_3 (mm)	0.0047	-0.0004	-0.0002
11	$\Delta\alpha_3$ (°)	0.1233	-0.0779	-0.0682
12	$\Delta\theta_3$ (°)	-1.9234	0.9971	0.9217
13	Δa_4 (mm)	-0.1235	-0.0497	-0.0418
14	Δd_4 (mm)	-0.3415	-0.0100	-0.0037
15	$\Delta\alpha_4$ (°)	-0.0222	0.0382	0.0373
16	$\Delta\theta_4$ (°)	2.3708	-0.0319	-0.0317
17	Trans(x, Δ_{SLM}) (mm)	0.0194	-0.0093	-0.0050
18	Trans(z, Δ_{SLM}) (mm)	0.3703	0.0004	0.0065
19	Rot(x, Δ_{SLM}) (°)	0.0644	-0.0155	-0.0118
20	Rot(y, Δ_{SLM}) (°)	0.5829	0.0135	0.0184
21	Rot(z, Δ_{SLM}) (°)	0.0156	0.0273	0.0219

$$
\begin{aligned}
{}^{\mathrm{SLM}}_{l_1}\mathbf{T} &= \mathrm{Rot}\,(x, -27.80^\circ)\,\mathrm{Rot}\,(y, 1.27^\circ) \\
{}^{\mathrm{SLM}}_{l_2}\mathbf{T} &= \mathrm{Rot}\,(x, 31.07^\circ)\,\mathrm{Rot}\,(y, 0.82^\circ)\,. \qquad (16)
\end{aligned}
$$

B. Results

Fig. 7 shows a snapshot of the manipulator and the two laser beams on the screen at the initial configuration, $(\theta_1, \theta_2, \theta_3, \theta_4) = (0.0^\circ, 0.0^\circ, 0.0^\circ, 0.0^\circ)$. Similar to the simulation, the laser positions of a total of 50 poses were measured, where the joint values for the first 25 poses were chosen between -10.0° and 10.0° and the others were chosen over the whole operating

TABLE VI
DISTANCE ERRORS OF TWO LASER BEAMS ON THE SCREEN BEFORE THE CALIBRATION PROCEDURE (EXPERIMENT)

	Calibration Set (mm)							Testing Set (mm)						
		l_1			l_2				l_1			l_2		
	Poses	Mean	STD	Max	Mean	STD	Max	Poses	Mean	STD	Max	Mean	STD	Max
Case 1	25	7.09	0.79	8.72	8.18	1.74	13.38	25	8.43	3.62	21.61	10.00	5.30	23.73
Case 2	25	8.07	3.53	21.61	9.19	3.97	20.17	25	7.40	1.20	9.76	8.92	3.99	23.73
Case 3	50	7.74	2.66	21.61	9.06	3.98	23.73	-	-	-	-	-	-	-

TABLE VII
DISTANCE ERRORS OF TWO LASER BEAMS ON THE SCREEN AFTER THE CALIBRATION PROCEDURE (EXPERIMENT)

		Calibration Set (mm)							Testing Set (mm)						
			l_1			l_2				l_1			l_2		
		Poses	Mean	STD	Max	Mean	STD	Max	Poses	Mean	STD	Max	Mean	STD	Max
EKF	Case 1	25	0.85	0.37	1.52	0.87	0.64	2.42	25	2.62	2.96	12.04	6.19	4.60	16.26
	Case 2	25	1.44	0.81	3.42	2.85	2.27	8.95	25	1.23	0.45	2.22	2.11	1.92	8.67
	Case 3	50	1.10	0.61	2.89	1.95	1.89	9.57	-	-	-	-	-	-	-

workspace shown in Table IV. Similarly, the calibration set contained only the poses covering a small range of workspace in Case 1, where Case 2 included the poses covering the whole workspace. In Case 3, all measured poses were used as the calibration set. Table VI shows the distance errors of the two laser beams on the screen for each case before the calibration procedure. The average distance errors of the calibration set for all three cases were similar, but the standard deviation value for Case 2 was higher than Case 1. In other words, the distance error value increased when the calibration set contained the poses covering the whole workspace.

Table V shows the estimated error values of the kinematic parameters when the calibration sets were used in EKF for 10 000 iterations. Table VII compares the distance errors of the two laser beams when the estimated error values were applied to the nominal D–H parameters. Since the simulation results confirmed that EKF was a better parameter estimation algorithm compared to LSE, EKF was only applied in the experimental model. After the kinematic calibration, the mean values of the calibration set for all three cases significantly decreased. They were smaller than the diffraction length of the laser beam, which was 4.0 mm. Similar to the simulation results, the results of the testing set in both Case 1 and Case 2 confirmed that the distance errors between the theoretical and measured positions of the two laser beams were decreased when the calibration set included the poses, which covered the whole operating workspace. Both the simulation and the experimental results confirmed that the proposed algorithm allowed us to estimate the entire kinematic parameter errors with the small number of poses measured in the operating workspace.

When the position of end-effector was only considered instead of the velocity at which the end-effector moves, the final error of the estimated D–H parameters was only minimized in the measured configurations, whereas this value became larger in different configurations [19]. In order to move the end-effector in a specified direction at a specified speed with accuracy, the motion of the individual joints must be coordinated. In this paper, the differential relationship between the joint displacements and the location of the SLM including its position and orientation was represented as the Jacobian matrix, and the variances between actual and measured positions of laser beams that influence the direction and speed of the SLM were used to estimate accurate kinematic parameters of the manipulator.

VI. CONCLUSION

This paper proposed the kinematic parameter estimation technique by utilizing an SLM and a stationary camera. The concept of differential kinematics was applied to relate the motion of individual links to the end-effector. Then, the relationship between the end-effector and the laser beamed on the screen was derived as Jacobian matrices. The multiple of these two Jacobian matrices allowed us to formulate a nonsingular Jacobian matrix that represents the relationship between all the kinematic parameters and the measured positions of laser beams on the screen. EKF was employed as an optimization tool to find the physical errors of kinematic parameters. Consequently, simulation and experimental results confirmed that the proposed technique allowed us to estimate the entire kinematic parameter errors with the small number of configurations. Verifying the effectiveness of the proposed kinematic calibration technique in other parameter optimization algorithms including evolutionary algorithm is left as a further work.

REFERENCES

[1] K. Harada, S. Hattori, H. Hirukawa, M. Morisawa, S. Kajita, and E. Yoshida, "Two-stage time-parametrized gait planning for humanoid robots," *IEEE/ASME Trans. Mechatronics*, vol. 15, no. 5, pp. 694–703, Oct. 2010.

[2] Y.-D. Hong, B.-J. Lee, and J.-H. Kim, "Command state-based modifiable walking pattern generation on an inclined plane in pitch and roll directions for humanoid robots," *IEEE/ASME Trans. Mechatronics*, vol. 16, no. 4, pp. 783–789, Aug. 2011.

[3] M. Piccigallo, U. Scarfogliero, C. Quaglia, G. Petroni, P. Valdastri, A. Menciassi, and P. Dario, "Design of a novel bimanual robotic system for single-port laparoscopy," *IEEE/ASME Trans. Mechatronics*, vol. 15, no. 6, pp. 871–878, Dec. 2010.

[4] R. Oshima, T. Takayama, T. Omata, K. Kojima, K. Takase, and N. Tanaka, "Assemblable three-fingered nine-degrees-of-freedom hand for laparoscopic surgery," *IEEE/ASME Trans. Mechatronics*, vol. 15, no. 6, pp. 862–870, Dec. 2010.

[5] Z. Roth, B. Mooring, and B. Ravani, "An overview of robot calibration," *IEEE J. Robot. Autom.*, vol. RA-3, no. 5, pp. 377–385, Oct. 1987.

[6] B. Mooring, Z. Roth, and M. Driels, *Fundamentals of Manipulator Calibration*. New York: Wiley, 1991.

[7] Z. Zhuang and Z. Roth, *Camera-Aided Robot Calibration*. Boca Raton, FL: CRC Press, 1996.

[8] J. Hollerbach and C. Wampler, "The calibration index and taxonomy for robot kinematic calibration methods," *Int. J. Robot. Res.*, vol. 15, pp. 573–591, 1996.
[9] G. Alici and B. Shirinzadeh, "Enhanced stiffness modeling, identification and characterization for robot manipulators," *IEEE Trans. Robot.*, vol. 21, no. 4, pp. 554–564, Aug. 2005.
[10] W. Newman, C. Birkhimer, and R. Horning, "Calibration of a motoman P8 robot based on laser tracking," in *Proc. IEEE Int. Conf. Robot. Autom.*, San Francisco, CA, Apr. 2000, pp. 3597–3602.
[11] A. Omodei, G. Legnani, and R. Adamini, "Three methodologies for the calibration of industrial manipulators: Experimental results on a SCARA robot," *J. Robot. Syst.*, vol. 17, no. 6, pp. 291–307, 2000.
[12] A. Omodei, G. Legnani, and R. Adamini, "Calibration of a measuring robot: Experimental results on a 5 DOF structure," *J. Robot. Syst.*, vol. 18, no. 5, pp. 237–250, 2001.
[13] G. Alici and B. Shirinzadeh, "A systematic technique to estimate positioning errors for robot accuracy improvement using laser interferometry based sensing," *Mech. Mach. Theory*, vol. 40, pp. 879–906, 2005.
[14] G. Alici, R. Jagielski, Y. Sekercioglu, and B. Shirinzadeh, "Prediction of geometric errors of robot manipulators with particle swarm optimization method," *Robot. Auton. Syst.*, vol. 54, pp. 956–966, 2006.
[15] J. O'Brian, R. Bodenheimer, G. Brostow, and J. Hodgins, "Automatic joint parameter estimation from magnetic motion capture data," in *Proc. Graph. Interface*, May 2000, pp. 53–60.
[16] P. Renaud, N. Andreff, J.-H. Lavest, and M. Dhome, "Simplifying the kinematic calibration of parallel mechanisms using vision-based metrology," *IEEE Trans. Robot.*, vol. 22, no. 1, pp. 12–22, Feb. 2006.
[17] A. Rauf, A. Pervez, and J. Ryu, "Experimental results on kinematic calibration of parallel manipulators using a partial pose measurement device," *IEEE Trans. Robot.*, vol. 22, no. 2, pp. 379–384, Apr. 2006.
[18] G. Gatti and G. Danieli, "A practical approach to compensate for geometric errors in measuring arms: Application to a six-degree-of-freedom kinematic structure," *Meas. Sci. Technol.*, vol. 19, no. 1, pp. 015107-10–015107-12, 2008.
[19] J. Santolaria, J. Aguilar, J. Yague, and J. Pastor, "Kinematic parameter estimation technique for calibration and repeatability improvement of articulated arm coordinate measuring machines," *Precis. Eng.*, vol. 32, pp. 251–268, 2008.
[20] S. Ye, Y. Wang, Y. Ren, and D. Li, "Robot calibration using iteration and differential kinematics," *J. Phys.: Conf. Series*, vol. 48, pp. 1–6, 2006.
[21] C. C. Iurascu and F. C. Park, "Geometric algorithms for kinematic calibration of robots containing closed loops," *J. Mech. Design*, vol. 125, pp. 23–32, 2003.
[22] J. Jang, S. Kim, and Y. Kwak, "Calibration of geometric and non-geometric errors of an industrial robot," *Robotica*, vol. 19, pp. 311–321, 2001.
[23] M. Varziri and L. Notash, "Kinematic calibration of a wire-actuated parallel robot," *Mech. Mach. Theory*, vol. 42, pp. 960–976, 2007.
[24] D. Daney, Y. Papegay, and B. Madeline, "Choosing measurement poses for robot calibration with the local convergence method and tabu search," *Int. J. Robot. Res.*, vol. 24, no. 6, pp. 501–518, 2005.
[25] J. Denavit and R.S. Hartenberg, "A kinematic notation for lower-pair mechanisms based on matrices," *Trans. ASME, J. Appl. Mech.*, vol. 22, pp. 215–221, 1955.
[26] A. H. Jazwinski, *Stochastic Processes and Filtering Theory*. San Diego, CA: Academic, 1970.
[27] H. W. Sorenson, *Kalman Filtering: Theory and Application*. Piscataway, NJ: IEEE Press, 1985.
[28] P. J. McKerrow, *Introduction to Robotics*. Sydney, Australia: Addison-Wesley, 1991.

In-Won Park received the B.S. degree in electrical engineering from the University of Toronto, Toronto, ON, Canada, in 2005. He is currently working toward the M.S.–Ph.D. joint degree in electrical engineering at Korea Advanced Institute of Science and Technology (KAIST), Daejeon, Korea.

His current research interests include the area of humanoid robotics, especially in kinematic calibration and optimal control.

Bum-Joo Lee received the B.S. degree in electrical engineering from Yonsei University, Seoul, Korea, in 2002, and the M.S. and Ph.D. degrees in electrical engineering from Korea Advanced Institute of Science and Technology (KAIST), Daejeon, Korea, in 2004 and 2008, respectively.

He is currently a Senior Engineer in the Digital Media and Communications R&D Center, Samsung Electronics, Suwon, Korea. His main research interests include the area of humanoid robotics, especially in generating dynamic walking gates.

Se-Hyoung Cho received the B.S. degree in electronic and electrical engineering from the University of Seoul, Seoul, Korea, in 2004, and the M.S. degree in electrical engineering from Korea Advanced Institute of Science and Technology (KAIST), Daejeon, Korea, in 2007, where he is currently working toward the Ph.D. degree.

His current research interests include humanoid robotics, evolvable artificial creatures, and ubiquitous robotics.

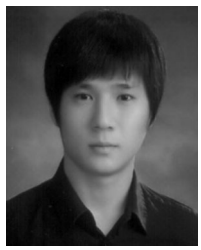

Young-Dae Hong received the B.S. and M.S. degrees in electrical engineering from Korea Advanced Institute of Science and Technology (KAIST), Daejeon, Korea, in 2007 and 2009, respectively, where he is currently working toward the Ph.D. degree.

His current research interests include the area of humanoid robotics, especially in footstep planning and walking pattern generation.

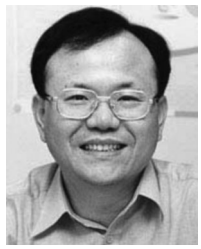

Jong-Hwan Kim (F'09) received the B.S., M.S., and Ph.D. degrees in electronics engineering from Seoul National University, Seoul, Korea, in 1981, 1983, and 1987, respectively.

Since 1988, he has been with the Department of Electrical Engineering, Korea Advanced Institute of Science and Technology (KAIST), Daejeon, Korea, where he is currently a Professor and Director of the National Robotics Research Center for Robot Intelligence Technology. His current research interests include the areas of ubiquitous and genetic robotics.

Dr. Kim currently serves as an Associate Editor of the IEEE TRANSACTIONS ON EVOLUTIONARY COMPUTATION, the *IEEE Computational Intelligence Magazine*, and the *International Journal of Social Robotics*. He was one of the cofounders of the International Conference on Simulated Evolution and Learning. He was the General Chair for the 2001 IEEE Congress on Evolutionary Computation held in Seoul, Korea. His name was included in *The Barons 500: Leaders for the New Century* in 2000 as the Father of Robot Football. He is the Founder of The Federation of International Robosoccer Association (FIRA, www.FIRA.net) and The International Robot Olympiad Committee (IROC, www.IROC.org). He is currently *serving* as the President of the FIRA and IROC.